Characterization of the O_2-Evolving Reaction Catalyzed by $[(terpy)(H_2O)Mn^{III}(O)_2Mn^{IV}(OH_2)(terpy)](NO_3)_3$ (terpy = 2,2′:6,2″-Terpyridine)

Julian Limburg,[‡,||] John S. Vrettos,[‡] Hongyu Chen,[‡] Julio C. de Paula,[§] Robert H. Crabtree,*[,‡] and Gary W. Brudvig*[,‡]

Contribution from the Department of Chemistry, Yale University, P.O. Box 208107, New Haven, Connecticut, 06520-8107, and Department of Chemistry, Haverford College, 370 Lancaster Ave., Haverford, Pennsylvania, 19041

Received March 28, 2000

Abstract: The complex $[(terpy)(H_2O)Mn^{III}(O)_2Mn^{IV}(OH_2)(terpy)](NO_3)_3$ (terpy = 2,2′:6,2″-terpyridine) (**1**) catalyzes O_2 evolution from either $KHSO_5$ (potassium oxone) or NaOCl. The reactions follow Michaelis−Menten kinetics where $V_{max} = 2420 \pm 490$ mol O_2 (mol **1**)$^{-1}$ hr^{-1} and $K_M = 53 \pm 5$ mM for oxone ([**1**] = 7.5 μM), and $V_{max} = 6.5 \pm 0.3$ mol O_2 (mol **1**)$^{-1}$ hr^{-1} and $K_M = 39 \pm 4$ mM for hypochlorite ([**1**] = 70 μM), with first-order kinetics observed in **1** for both oxidants. A mechanism is proposed having a preequilibrium between **1** and HSO_5^- or OCl^-, supported by the isolation and structural characterization of $[(terpy)(SO_4)Mn^{IV}(O)_2Mn^{IV}(O_4S)(terpy)]$ (**2**). Isotope-labeling studies using $H_2{}^{18}O$ and $KHS^{16}O_5$ show that O_2 evolution proceeds via an intermediate that can exchange with water, where Raman spectroscopy has been used to confirm that the active oxygen of HSO_5^- is nonexchanging ($t_{1/2} \gg 1$ h). The amount of label incorporated into O_2 is dependent on the relative concentrations of oxone and **1**. $^{32}O_2$:$^{34}O_2$:$^{36}O_2$ is 91.9 ± 0.3:7.6 ± 0.3:0.51 ± 0.48, when $[HSO_5^-] = 50$ mM (0.5 mM **1**), and 49 ± 21:39 ± 15:12 ± 6 when $[HSO_5^-] = 15$ mM (0.75 mM **1**). The rate-limiting step of O_2 evolution is proposed to be formation of a formally Mn^V═O moiety which could then competitively react with either oxone or water/hydroxide to produce O_2. These results show that **1** serves as a functional model for photosynthetic water oxidation.

Introduction

The oxygen-evolving complex (OEC) of photosystem II (PS II) contains a μ-oxo-bridged manganese tetramer that can carry out the four-electron oxidation of water to O_2.[1−8] The key intermediate has been postulated as a Mn═O species formed by the abstraction of H-atoms from a water ligated to manganese by a tyrosyl radical.[2−4,9−11] O−O bond formation could then involve the reaction of a second molecule of water with the terminal oxo ligand.[1−3,12,13]

Bioinorganic model chemistry has provided important insights into the mechanism of photosynthetic water oxidation, in particular by inspiring the aforementioned idea that a Mn═O species is involved.[7,13−15] Several studies give credence to this proposal. $[(bpy)_2(H_2O)Ru^{III}(O)Ru^{III}(OH_2)(bpy)_2]^{4+}$ (bpy = 2,2′-bipyridine)[16−18] and related complexes have been shown to oxidize water via a Ru═O intermediate.[19] A di-manganese diporphyrin complex has been reported that can oxidize water electrochemically, with a Mn═O species proposed to be the reactive intermediate.[20] Such an assignment is supported by mechanistic studies on Mn−porphyrin oxidation catalysts where this intermediate has been observed,[21,22] and there are a series of structurally characterized, albeit relatively unreactive, Mn═O

* To whom correspondence should be addressed: Telephone: (203)-432-5202 (GWB), (203)-432-3925 (R.H.C.). Fax: (203)-432-6144 (G.W.B., R.H.C.). E-mail: gary.brudvig@yale.edu, robert.crabtree@yale.edu.

‡ Yale University.

§ Haverford College.

|| Current address: Department of Chemistry, University of California at Berkeley, Berkeley, California, 94704.

(1) Vrettos, J. S.; Limburg, J.; Brudvig, G. W. *Biochim. Biophys. Acta* **2001**, *1503*, 229−245.

(2) Limburg, J.; Brudvig, G. W.; Crabtree, R. H. In *Biomimetic Oxidation Chemistry*; Meunier, B., Ed.; World Scientific: Singapore, 2000; pp 509−541.

(3) Limburg, J.; Szalai, V. A.; Brudvig, G. W. *J. Chem. Soc., Dalton Trans.* **1999**, 1353−1363.

(4) Britt, R. D. In *Oxygenic Photosynthesis: The Light Reactions*; Ort, D. R., Yocum, C. F., Eds.; Advances in Photosynthesis, Vol. 4; Kluwer Academic Publishers: Dordrecht, The Netherlands, 1996; pp 137−159.

(5) Debus, R. J. *Biochim. Biophys. Acta* **1992**, *1102*, 269−352.

(6) Penner-Hahn, J. E. *Struct.Bonding* **1998**, *90*, 1−36.

(7) Rüttinger, W.; Dismukes, G. C. *Chem. Rev.* **1997**, *97*, 1−24.

(8) Yachandra, V. K.; Sauer, K.; Klein, M. P. *Chem. Rev.* **1996**, *96*, 2927−2950.

(9) Hoganson, C. W.; Lydakis-Simantiris, N.; Tang, X.-S.; Tommos, C.; Warncke, K.; Babcock, G. T.; Diner, B. A.; McCracken, J.; Styring, S. *Photosynth. Res.* **1995**, *46*, 177−184.

(10) Hoganson, C. W.; Babcock, G. T. *Science* **1997**, *277*, 1953−1956.

(11) Messinger, J.; Badger, M.; Wydrzynski, T. *Proc. Natl. Acad. Sci. U.S.A.* **1995**, *92*, 3209−3213.

(12) Siegbahn, P. E. M.; Crabtree, R. H. *J. Am. Chem. Soc.* **1995**, *117*, 7−127.

(13) Pecoraro, V. L.; Baldwin, M. J.; Caudle, M. T.; Hsieh, W.; Law, N. A. *Pure Appl. Chem.* **1998**, *70*, 925−929.

(14) Limburg, J.; Vrettos, J. S.; Liable-Sands, L. M.; Rheingold, A. L.; Crabtree, R. H.; Brudvig, G. W. *Science* **1999**, *283*, 1524−1527.

(15) Limburg, J.; Brudvig, G. W.; Crabtree, R. H. *J. Am. Chem. Soc.* **1997**, *119*, 2761−2762.

(16) Geselowitz, D.; Meyer, T. J. *Inorg. Chem.* **1990**, *29*, 3894−3896.

(17) Gersten, S. W.; Samuels, G. J.; Meyer, T. J. *J. Am. Chem. Soc.* **1982**, *104*, 4029−4030.

(18) Binstead, R. A.; Chronister, C. W.; Ni, J. F.; Hartshorn, C. M.; Meyer, T. J. *J. Am. Chem. Soc.* **2000**, *122*, 8464−8473.

(19) Hurst, J. K.; Zhou, J.; Lei, Y. *Inorg. Chem.* **1992**, *31*, 1010−1017.

(20) Naruta, Y.; Sasayama, M.; Sasaki, T. *Angew. Chem., Int. Ed. Engl.* **1994**, *33*, 1839−1841.

(21) Groves, J. T.; Stern, M. K. *J. Am. Chem. Soc.* **1988**, *110*, 8628−8638.

10.1021/ja001090a CCC: $20.00
Published on Web 12/28/2000

complexes.[23−28] These studies give support to the idea that a Mn═O species is involved in the water-oxidation chemistry of the OEC.

It has been proposed that a Mn═O intermediate can exchange with H_2O via an oxo/hydroxo tautomeric mechanism.[29,30] In this way, incorporation of isotopically labeled $H_2{}^{18}O$ into oxidized organic products has been used as a mechanistic probe when studying Mn−porphyrin oxidation catalysis.[21,22,29−31] An important caveat of this method is that the primary oxidant must be slow to exchange with free water relative to its rate of reaction with the catalyst.[32]

Recently, we reported a reaction of OCl^- with the complex $[(terpy)(H_2O)Mn^{III}(O)_2Mn^{IV}(OH_2)(terpy)]^{3+}$ (**1**) (terpy = 2,2′:6,2″-terpyridine) as a catalyst, that resulted in the catalytic formation of O_2, but **1** was deactivated by the irreversible formation of permanganate.[14] This was the first report of a di-μ-oxo dimanganese complex, a structural model for the manganese complex in the OEC, that could carry out catalytic O−O bond formation. The mechanism proposed for this functional model for the OEC involves formation of O_2 by reaction of a formally Mn^V═O intermediate with outer sphere water/hydroxide. Complementary to the use of OCl^-, we have also studied the O_2-evolving reaction of HSO_5^- with Mn(II) using dpa (dpa = dipicolinate)[15,33] and terpy, where mixed-valence di-μ-oxo dimers formed in situ.[15] Control experiments using Lewis acids (Zn^{2+} and Al^{3+}), where no reactivity was observed, showed that the O_2-evolving reaction of HSO_5^- did not involve Lewis acid-promoted hydrolysis to form H_2O_2 followed by its dismutation.[15]

In this paper, we compare the mechanisms of the catalytic O_2-evolving reactions between **1** and the oxygen-atom transfer reagents HSO_5^- (potassium oxone) and OCl^- (both referred to as XO). The similarity of the kinetics observed when using oxone versus hypochlorite suggests that the two oxidants employ analogous mechanisms in their reactions with **1**. We propose that the key intermediate is a Mn═O species, as suggested in our previous reports. Kinetic and isotopic labeling studies support a mechanism in which a Mn═O intermediate forms following the reversible binding of XO to **1**. We have isolated and structurally characterized the complex $[(terpy)(SO_4)Mn^{IV}(O)_2Mn^{IV}(O_4S)(terpy)]$ (**2**)[14] as a model for the binding of oxone to **1**. The results reported here support our assignment of **1** as a functional model of photosynthetic water oxidation.[14]

Table 1. Crystal Data and Structure Refinement for **2**·6H_2O

	2·6H_2O
chemical formula	$C_{30}H_{34}N_6O_{16}S_2Mn_2$
formula weight	908.63
crystal system	monoclinic
space group (no.)	*C*2/*c* (15)
a (Å)	27.091(4)
b (Å)	9.036(2)
c (Å)	18.281(5)
β (deg)	127.42(2)
V (Å^3)	3554(1)
T (°C)	−90.0
λ (Å)	0.71069
δ_{calc} (g cm^{-3})	1.675
Z	4
F(000)	1816.00
abs coeff, cm^{-1}	9.11
no. of reflecns collcd/unique	3955/3834
no. of observations ($I > 3\sigma(I)$)	1323
no. of refined params	253
largest peak/hole, e Å^{-1}	0.53/−0.45
R^a	0.055
$R_w{}^b$	0.056
goodness of fit indicator	1.58

$^a R = \Sigma||F_o| - |F_c||/\Sigma|F_o|$. $^b R_w = [(\Sigma w(|F_o| - |F_c|)^2/\Sigma w F_o{}^2)]^{1/2}$.

Experimental Section

All solutions were prepared using doubly deionized water. $H_2{}^{18}O$ (85.5 atom %) was purchased from ICON Stable Isotopes. All other chemicals were purchased from Aldrich and used without further purification. NaOCl (10−13%) and $KHSO_5$ were standardized using iodometric titrations. All oxone solutions were made up in acetate buffer (0.23 M $HOAc/OAc^-$, pH = 4.5), and all hypochlorite solutions were adjusted to pH = 8.6 using concentrated HNO_3. **1** was synthesized as reported previously.[14,34]

Synthesis of $[(terpy)(SO_4)Mn^{IV}(O)_2Mn^{IV}(O_4S)(terpy)]$. To a stirring solution of $MnSO_4$ (73 mg, 0.429 mmol) and 2,2′:6′,2″-terpyridine (100 mg, 0.429 mmol) in nitric acid (10 mL, pH = 2) was added potassium peroxomonosulfate (111 mg, 0.322 mmol) in nitric acid (3 mL, pH = 2). The yellow solution turned green and then brown/red. After stirring for 10 min, the mixture was transferred to a beaker and left to evaporate at room temperature. After 48 h, crystals of **2** had formed as dark red plates, and these were filtered on a frit and washed with a small volume of iced water and then copious acetonitrile. Yield = 84 mg (44%). Analysis $C_{30}H_{22}N_6O_{16}S_2Mn_2$, **2**·3$H_2O$ calculated: C 42.15%, H 3.28%, N 9.84%, S 7.50%; found: C 42.02%, H 3.29%, N 9.84%, S 7.50%; IR (KBr): 3460 (s, br), 1605 (m), 1571 (m), 1477 (m), 1193 (m), 1179 (m), 1026 (s), 791 (m), 687 (m), 662 (m). The UV/vis spectrum of **2** has been published previously.[14]

Crystal Structure Determination of 2. A crystal of **2** of dimensions 0.09 × 0.17 × 0.22 mm was taken directly from the reaction mixture. Diffraction data were collected on an Enraf-Nonius CAD-4 diffractometer with graphite monochromated Mo Kα radiation, and the crystallographic data are summarized in Table 1.

The structure of **2** was solved by heavy-atom Patterson methods,[35] and expanded using Fourier techniques. The non-hydrogen atoms were refined anisotropically, and hydrogen atoms were included but not refined.[36] All calculations were performed using teXsan.[37] The full details of the X-ray structure determination can be found in the Supporting Information.

O_2 Evolution. Initial rates of O_2 evolution were measured with a YSI Standard Oxygen Probe (Clark electrode) attached to a Cole-Palmer chart recorder. In a typical experiment an aliquot (10−50 μL) of a solution of **1** (1−5 mM) was added to a 4 mL solution of either oxone

(22) Groves, J. T.; Lee, J.; Marla, S. S. *J. Am. Chem. Soc.* **1997**, *119*, 6269−6273.
(23) Collins, T. J.; Gordon-Wylie, S. W. *J. Am. Chem. Soc.* **1989**, *111*, 4511−4513.
(24) Collins, T. J.; Powell, R. D.; Slebodnick, C.; Uffelman, E. S. *J. Am. Chem. Soc.* **1990**, *112*, 899−901.
(25) Collins, T. J. *Acc. Chem. Res.* **1994**, *27*, 279−285.
(26) Miller, C. G.; Gordon-Wylie, S. W.; Horwitz, C. P.; Strazisar, S. A.; Peraino, D. K.; Clark, G. R.; Weintraub, S. T.; Collins, T. J. *J. Am. Chem. Soc.* **1998**, *120*, 11540−11541.
(27) MacDonnell, F. M.; Fackler, N. L. P.; Stern, C.; O'Halloran, T. V. *J. Am. Chem. Soc.* **1994**, *116*, 7431−7432.
(28) Shirin, Z.; Hammes, B. S.; Young, V. G., Jr.; Borovik, A. S. *J. Am. Chem. Soc.* **2000**, *122*, 1836−1837.
(29) Bernadou, J.; Fabiano, A.-S.; Robert, A.; Meunier, B. *J. Am. Chem. Soc.* **1994**, *116*, 9375−9376.
(30) Bernadou, J.; Meunier, B. *J. Chem. Soc., Chem. Commun.* **1998**, 2167−2173.
(31) Groves, J. T.; Stern, M. K. *J. Am. Chem. Soc.* **1987**, *109*, 3812−3814.
(32) Nam, W.; Valentine, J. S. *J. Am. Chem. Soc.* **1993**, *115*, 1772−1778.
(33) Limburg, J.; Crabtree, R. H.; Brudvig, G. W. *Inorg. Chim. Acta* **2000**, *297*, 301−306.
(34) Collomb, M.-N.; Deronzier, A.; Richardot, J.; Pecaut, J. *New J. Chem* **1999**, *23*, 351−353.
(35) Beurskens, P. T.; Admiraal, G.; Beurskens, G.; Bosman, W. P.; Garcia-Granda, S.; Gould, R. O.; Smits, J. M. M.; Smykalla, C. PATTY: The DIRDIF program system, Techical Report of the Crystallography Laboratory; University of Nijmegen, 1992.

(5−200 mM) or hypochlorite (10−100 mM) which was being stirred beneath the electrode. All rates were measured at 25 °C using the method of initial rates by taking the recorded slope from $t = 0$ to $t =$ 30 s. Each rate reported is an average of at least three runs.

When higher concentrations of **1** (>0.1 mM) were added to a solution of oxone, the amount of O_2 evolved was too large to measure using a Clark electrode because bubbles were formed. In these cases, the volume of gas produced was measured by running the reaction in a 25 mL sidearm Erlenmeyer flask with a 1 m × 2.75 mm i.d. capillary tube attached to the sidearm, and a stopcock connected to the top. The typical volume of a solution was 5 mL, and the concentrations of oxone and **1** were as in the mass spectrometry experiments (see below). **1** was introduced to a stirring oxone solution through the stopcock, which was immediately closed. The volume of O_2 produced was measured by the displacement of a bead of glycerol present in the capillary tube.

Raman Measurements on the Rate of Exchange of the Active Oxygens in OCl^- and HSO_5^- with Water. Raman spectra were obtained with a SPEX Raman 500 equipped with a liquid nitrogen cooled CCD detector (ISA CCD-2000) using a Spectra Physics model 161B Ar-ion laser operating at 488 nm. Incident laser powers were between 8 and 10 mW; only the Raman intensities and no spectral features changed as a function of power. Rayleigh scatter from the 488 nm laser line was rejected by a custom-built Kaiser Optical Systems (Ann Arbor, MI) holographic notch filter. The detection geometry was 90° using a quartz cuvette. The exchange experiments were carried out by injecting 250 μL of either OCl^- (0.5 M) or HSO_5^- (0.5 M) reagent into the cuvette containing 250 μL of water (^{16}O or ^{18}O, final ^{18}O composition was 42.5 atom %) immediately before accumulating spectra. All experiments were reproduced at least twice. Spectra were fit to the sum of a baseline and Gaussian curves using Igor Pro (v. 3.14, WaveMetrics, Inc.).

Mass Spectrometry−^{18}O Labeling. An aqueous solution of **1** (50 μL, 5 mM in 0.1 M KNO_3, pH = 4.5)[34] and an aqueous solution of $KHS^{16}O_5$ (either 200 μL or 40 μL, 0.125 M) were placed in separate bulbs of a two-bulb flask (each bulb had a volume of ∼15 mL). $H_2{}^{18}O$ (250 μL, 85.5%) was then added to the solution of **1**, and both solutions were degassed via three freeze−pump−thaw cycles. The two solutions were then mixed under a 10 mTorr atmosphere of He, and O_2 evolution was allowed to occur for 1 h, at which time the solution was frozen and the headspace gas drawn up into an evacuated 150-mL metal cylinder. The gas was then analyzed using a HP 5989A mass spectrometer. Two measurements were taken at the higher oxone concentration and three at the lower.

The final ^{18}O content of the water was calculated from the ratio of the $^{46}CO_2$: $^{48}CO_2$ peaks, as the oxygens in CO_2 exchange rapidly ($t_{1/2}$ < 10 s) with solvent water. The amount of label incorporation into the O_2 evolved was then normalized to the ^{18}O content. The yield of $^{32}O_2$ was adjusted by subtracting the background amount of $^{32}O_2$ based on the amount of $^{28}N_2$ in each run to correct for incomplete degassing or background air. This correction was less than 3% for both of the runs at higher oxone concentration, and one of the lower oxone runs, but higher (∼70%) for the other two lower oxone runs. These corrections are reflected in the reported errors for the relative yields of $^{32}O_2$, $^{34}O_2$, and $^{36}O_2$.

Oxidizing Equivalents. The oxidizing equivalents of oxone remaining as a function of time were measured using the same initial concentrations of oxone and **1** as in the mass spectrometry experiments. Aliquots of the reaction solution were quenched by injected into solutions of KI and the amount of I_2/I_3^- produced was determined by titration with a standardized solution of sodium thiosulfate.

EPR Spectroscopy. Spectra were collected at 10 K on frozen samples with an X-band Varian E-9 spectrometer equipped with an Oxford ESR-900 liquid helium cryostat. Typical instrument settings were the following: modulation amplitude = 20 G, modulation frequency = 100 kHz, and microwave power = 0.5 mW. The amount of mixed-valence dimer was quantified by measuring the amplitude of the peak near 3300 G and comparing this value with an authentic sample of **1**.

UV−Visible Spectroscopy. UV/vis spectra were recorded on a HP 8452A Diode Array spectrophotometer. Reactions were run at 25 °C. A 1-mm path length cuvette was used to follow the spectra at the higher concentrations of oxone and **1** used for the mass spectrometry experiments, and a 1-cm path length cuvette used for the spectra collected under the Clark-electrode conditions.

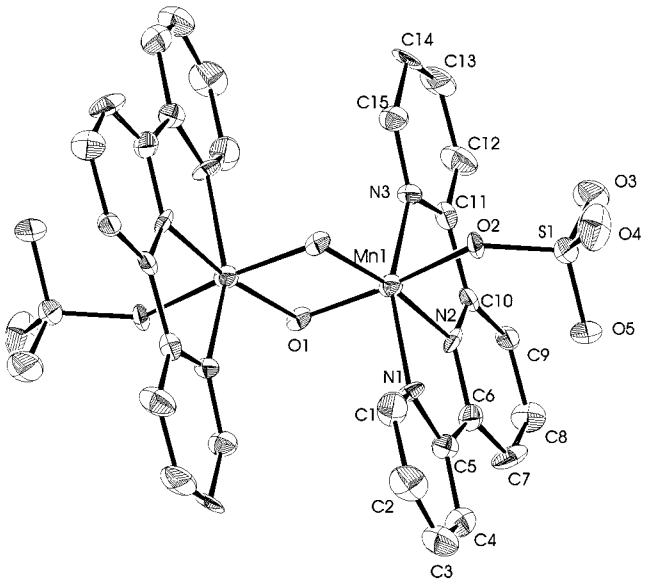

Figure 1. ORTEP diagram of **2**.

Table 2: Selected Bond Distances (Å) and Angles (deg) for **2**·6H_2O

Mn(1)−Mn(1)	2.769(3)	Mn(1)−O(1)	1.833(6)
Mn(1)−O(1)	1.794(6)	Mn(1)−O(2)	1.890(6)
Mn(1)−N(1)	2.009(7)	Mn(1)−N(2)	1.994(8)
Mn(1)−N(3)	2.035(7)		
Mn(1)−Mn(1)−O(1)	39.7(2)	Mn(1)−Mn(1)−O(1)	40.7(2)
Mn(1)−Mn(1)−O(2)	132.5(2)	Mn(1)−Mn(1)−N(1)	99.9(2)
Mn(1)−Mn(1)−N(2)	128.0(2)	Mn(1)−Mn(1)−N(3)	100.3(2)
O(1)−Mn(1)−O(1)	80.5(3)	O(1)−Mn(1)−O(2)	172.2(3)
O(1)−Mn(1)−N(1)	93.0(3)	O(1)−Mn(1)−N(2)	88.3(3)
O(1)−Mn(1)−N(3)	93.9(3)	O(1)−Mn(1)−O(2)	91.7(3)
O(1)−Mn(1)−N(1)	102.3(3)	O(1)−Mn(1)−N(2)	168.7(3)
O(1)−Mn(1)−N(3)	101.9(3)	O(2)−Mn(1)−N(1)	88.2(3)
O(2)−Mn(1)−N(2)	99.5(3)	O(2)−Mn(1)−N(3)	88.0(3)
N(1)−Mn(1)−N(2)	78.0(3)	N(1)−Mn(1)−N(3)	155.7(3)
N(2)−Mn(1)−N(3)	79.0(4)	Mn(1)−O(1)- -Mn(1)	99.5(3)
Mn(1)−O(2)−S(1)	133.4(4)	Mn(1)−N(1)−C(1)	122.5(7)

Results

Synthesis and Structure of [(terpy)(SO_4)Mn^{IV}($O)_2Mn^{IV}$-(O_4S)(terpy)] (2). In prior work, we had only been able to determine the structure of the mixed-valence III/IV form of the catalyst. Now, we find that the use of sulfate as a counterion allows the IV/IV form to be crystallographically characterized. Figure 1 shows the crystal structure of **2**, with bond distances and bond angles summarized in Table 2. The structure is very similar to that of the III/IV species and suggests that the cluster retains its identity on redox cycling. **2** forms by disproportionation from a solution containing the mixed-valence dimer, **1**, and SO_4^{2-}, and **2** was originally isolated from an attempt to make the mixed-valence dimer. The ligation of one doubly charged SO_4^{2-} group to each Mn has the effect of stabilizing the Mn^{IV} oxidation state, and **2** has no net charge. The Mn ions are separated by the ∼2.7 Å (Table 2) distance characteristic

(36) Beurskens, P. T.; Admiraal, G.; Beurskens, G.; Bosman, W. P.; de Gelder, R.; Israel, R.; Smits, J. M. M. DIRDIF-94: The DIRDIF-94 program system, Technical Report of the Crystallography Laboratory; University of Njimegen, 1994.

(37) *teXsan: Crystal Structure Analysis Package*; Molecular Structure Corporation, 1992.

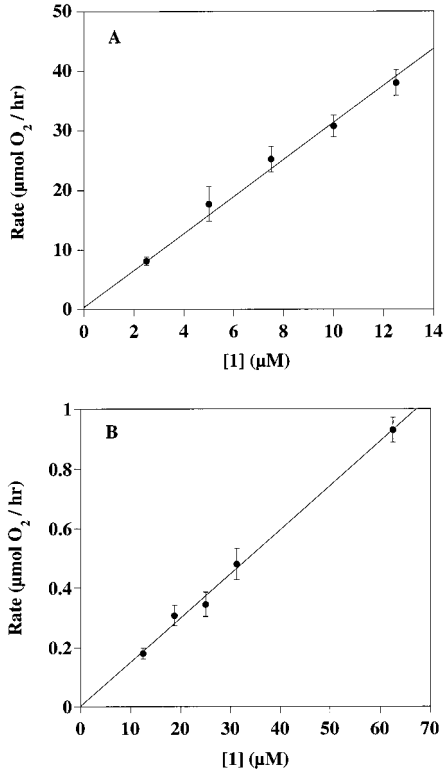

Figure 2. Plots showing the effect of varying [**1**] on the initial rates of O_2 evolution; (A) HSO_5^- (30 mM in 0.23 M HOAc/OAc^-, pH = 4.5), (B) OCl^- (70 mM, pH = 8.6). Errors reported are one standard deviation from the average of all runs carried out at each concentration.

of di-μ-oxo Mn dimers,[38,39] and which is virtually invariant between the $Mn^{III}Mn^{IV}$ and $Mn^{IV}{}_2$ complexes (d(Mn−Mn) is 2.723 Å in **1**[14,34] vs 2.769 Å in **2**). Unlike the III/IV dimer, **2** is EPR-silent, as expected for a strongly coupled Mn^{IV} dimer. Furthermore, the $Mn(O)_2Mn$ core vibrational frequencies downshift to lower energies on going from the mixed-valence[14,34] to the IV/IV dimer. The IR bands appear at 703 and 687 cm^{-1} in **1** and **2**, respectively, while in the Raman spectrum the complicated set of peaks over the range of 698, 671, 630, and 597 cm^{-1} downshifts to 652, 552, and 540 cm^{-1} due to the changes in both oxidation state and symmetry. These shifts are typical for di-μ-oxo Mn dimers.[38,39]

2 is only sparingly soluble in water, and dissolution is relatively slow when compared to that of **1**, presumably because the SO_4^{2-} ligands must be displaced by water. **2**, being a Mn^{IV} complex, would be expected to be relatively inert to ligand exchange as the Mn ions are high-spin d^3. The coordination of SO_4^{2-} provides support for the idea that the aqua ligand sites in **1** are exchangeable in solution as **2** forms from a solution of **1**, and this exchange is partly responsible for the catalytic activity **1**.

Initial Rates of O_2 Evolution. We have followed the effect of varying both **1** (Figure 2) and XO (Figure 3) on the initial rate of O_2 evolution, using pseudo-first-order conditions in substrate, and find results that suggest that Mn═O formation is rate-limiting for both OCl^- and HSO_5^-. The results of these experiments are summarized in Table 3. O_2 evolution is first-order in **1** and displays saturation kinetics when varying XO. These results are consistent with a mechanism that involves a preequilibrium between **1** and XO,[33] with the reaction of the **1**−XO complex so formed being the rate-limiting step.

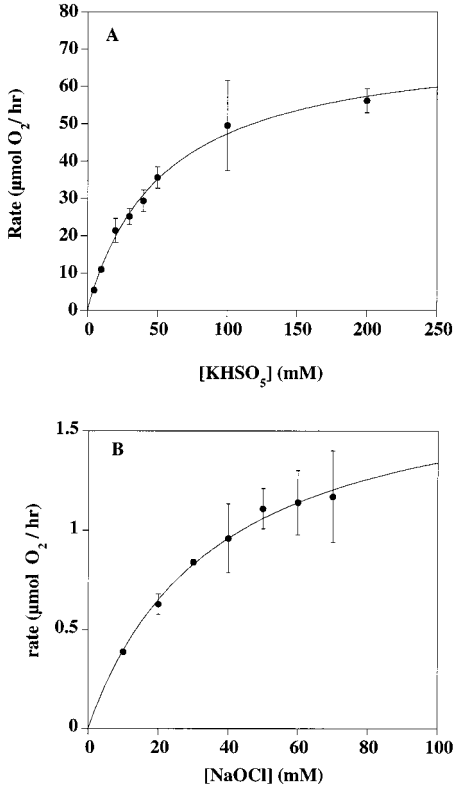

Figure 3. (A) Effect of varying [HSO_5^-] (0.23 M HOAc/OAc^-, pH = 4.5) on the initial rates of O_2 evolution ([**1**] = 7.5 μM). (B) Effect of varying [OCl^-] (pH = 8.6) in the initial rates of O_2 evolution ([**1**] = 70 μM). Both plots are fitted to the Michaelis−Menten equation. Errors reported are one standard deviation from the average of all runs carried out at each concentration.

Table 3: Kinetics Data Calculated from Figures 2 and 3

	HSO_5^-	OCl^-
order in **1**[a]	0.95 ± 0.06	1.00 ± 0.06
order in XO[b]	0.99 ± 0.02	0.70 ± 0.01
K_M[c](mM)	53 ± 5	36 ± 4
V_{max}[c] (mol O_2 (mol **1**)$^{-1}$ hr^{-1})	2420 ± 490	6.5 ± 0.3

[a] Calculated from a log rate vs log concentration plot of the data from Figure 2. [b] Calculated from a log rate vs log concentration plot of the data from Figure 3. [c] Calculated from the Michaelis−Menten fit of the data from Figure 3.

The V_{max} for O_2 evolution with HSO_5^- is nearly 400 times faster than for OCl^- (Table 3). The difference in rates may be due either to inherently greater reactivity on the part of oxone or may reflect the difference in the pH at which the two oxidants are used (pH = 4.5 for HSO_5^- and 8.6 for OCl^-). When dpa is used as a ligand in the oxone system, the O_2-evolving reaction is considerably slower at higher pH[15] and is accompanied by an increase in the rate of permanganate formation.[14,15,33] Oxone cannot be used at pH > 7 as it is decomposes directly to O_2 in basic solution.

Rates of Exchange of the Active Oxygens in $KHS^{16}O_5$ and $Na^{16}OCl$ with $H_2{}^{18}O$. It is of critical importance to establish whether the oxygens in the O_2 evolved from the reaction of **1** and XO arise from water or from the oxidant. This can be achieved using ^{18}O-isotope labeling of the water if the active O-atom of XO is slow ($t_{1/2}$ > 1 h) to exchange. Raman spectroscopy was chosen as a convenient and facile method for direct measurement of the exchange kinetics of both hypochlorite and oxone; this is the first application of this method.

(38) Manchanda, R.; Brudvig, G. W.; Crabtree, R. H. *Coord. Chem. Rev.* **1995**, *144*, 1−38.
(39) Thorp, H. H.; Brudvig, G. W. *New J. Chem.* **1991**, *15*, 479−490.

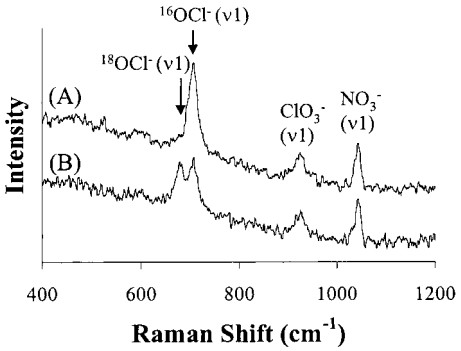

Figure 4. Raman spectra accumulated over the first 30 s after mixing 250 μL of OCl^- (0.5 M, pH = 8.6) with 250 μL of (A) $H_2{}^{16}O$ and (B) $H_2{}^{18}O$. The shift of the $^{18}OCl^-$ peak from the parent $^{16}OCl^-$ peak is indicated by the arrows. Each spectrum is an average of six scans integrated for 5 s with an incident laser power of 8 mW.

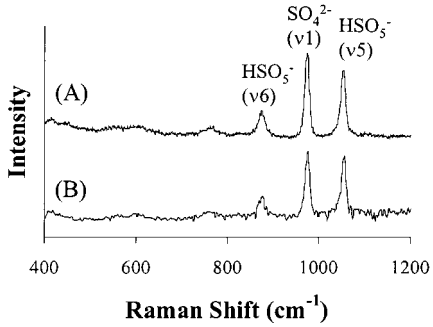

Figure 5. Raman spectra accumulated over the first 20 min after mixing 250 μL of HSO_5^- (0.5 M, pH = 4.5) with 250 μL of (A) $H_2{}^{16}O$ and (B) $H_2{}^{18}O$. Each spectrum is an average of six scans integrated for 5 s with an incident laser power of 8 mW.

Table 4: Results of the ^{18}O-Isotope-Labeling Experiments Showing the Percentage Yields of $^{32}O_2$, $^{34}O_2$, and $^{36}O_2$ from the Reaction between **1** and HSO_5^-

conditions	$^{32}O_2{}^{a,b}$ (%)	$^{34}O_2{}^{a}$ (%)	$^{36}O_2{}^{a}$ (%)
50 mM HSO_5^-, 0.5 mM **1**[c]	91.9 ± 0.3	7.6 ± 0.3	0.51 ± 0.48
15 mM HSO_5^-, 0.75 mM **1**[d]	49 ± 21	39 ± 15	12 ± 6

[a] Normalized to the concentration of $H_2{}^{18}O$; the errors are one standard deviation. [b] $^{32}O_2$ yields corrected for background air using $^{28}N_2$. [c] Average of two runs. [d] Average of three runs.

Hypochlorite/Solvent Exchange. Using indirect methods we[14] and others[40,41] had found OCl^- to be an apparently slow exchanger, but a direct measurement using ^{17}O NMR showed that in reality OCl^- exchanges rapidly ($t_{1/2}$ < 20 s).[42] These contrasting results led us to reexamine the exchange kinetics of OCl^-.[43]

The Raman spectra of hypochlorite recorded over the first 30 s after mixing with $H_2{}^{16}O$ and $H_2{}^{18}O$ are shown in Figure 4. In Figure 4A, besides the $^{16}OCl^-$ peak at 708 cm^{-1}, the ν1 modes of NO_3^- (1045 cm^{-1}) and ClO_3^- (930 cm^{-1}) are observed.[44] Figure 4B shows that within the first 30 s after mixing with $H_2{}^{18}O$, the exchange of the O-atom in OCl^- with solvent is complete. The $^{18}OCl^-$ peak downshifts 23 cm^{-1} to 685 cm^{-1},[44] as indicated by the arrows. The final isotopic composition of the water is 42.5% ^{18}O/57.5% ^{16}O, which is reflected in the ratio of the areas of the $^{18}OCl^-/^{16}OCl^-$ peaks (0.74 expected, 0.77 calculated). The NO_3^- and ClO_3^- peaks do not shift over the first 10 min (data not shown).

These data show that the O-atom exchange of OCl^- with water is indeed fast, as previously reported.[42,43] Equilibrium is reached within the first 30 s, indicating that the half-life must be $t_{1/2}$ < 10 s. This makes OCl^- unsuitable for use in the ^{18}O-labeling experiments.

Oxone/Solvent Exchange. Having confirmed that hypochlorite exchanges rapidly, oxone became the obvious choice of oxidant for the isotope-labeling experiments. Peroxides (e.g., H_2O_2 or *m*-chloroperoxybenzoic acid) are intrinsically inert to exchange with water,[32] and oxone has been shown to follow this trend.[29,31,45] However, there have been no studies using a direct spectroscopic measurement. Figure 5, A and B, show the spectra of oxone recorded over the first 20 min after mixing with $H_2{}^{16}O$ and $H_2{}^{18}O$, respectively. The peak at 980 cm^{-1} arises from the symmetric stretch of SO_4^{2-}, which is present in potassium oxone.[44,46] Sulfate has been shown by mass spectrometry to exchange slowly with water,[47] which our results support. The peroxy mode of oxone appears at 878 cm^{-1} (ν6) and the S=O stretch at 1055 cm^{-1} (ν5).[48−50] As shown in Figure 5B, there is no ^{18}O incorporation after 20 min, nor was any exchange observed even after more than 1 h (not shown). This is the first direct observation that oxone is slow to exchange with water, confirming the previous conclusions based on indirect studies of organic oxidation products.[29,31,45]

^{18}O Labeling. As oxone is slow to exchange with solvent water, the source of the O-atoms in the O_2 evolved from the catalytic reaction, H_2O versus HSO_5^-, could be ascertained using ^{18}O-labeled water. The results are summarized in Table 4. Initially the reaction was run under a relatively high concentration of oxone to maximize the yield of O_2. Under these conditions, about 8% of the O_2 evolved contained a single label ($^{34}O_2$), and only a very small amount of doubly labeled product ($^{36}O_2$) was observed. Lowering the oxone to **1** ratio by 5-fold caused a dramatic increase of labeled O_2 to approximately 50%, with a significant amount of $^{36}O_2$ observed. These results are consistent with the formation of a reactive intermediate that can exchange with solvent water and suggest that there is more than one pathway for O−O bond formation. Most importantly, these results cannot be explained by a mechanism where ^{18}O-exchange involves free oxone, and so all the $^{36}O_2$ and some of the $^{34}O_2$ must result from water oxidation.

O_2 Evolution Under Limiting Oxone Conditions. To understand why ^{18}O incorporation into O_2 was greatest under limiting oxone conditions, we have studied the kinetics of the oxone reaction under these conditions. Figure 6 shows the volume of O_2 gas evolved as a function of time (in both H_2O and D_2O). The mass spectrometry data on the reaction show that O_2 is the only gaseous product. Inspection of Figure 6

(40) Anwar, M.; Taube, H. *J. Am. Chem. Soc.* **1958**, *80*, 1073−1077.
(41) Meunier, B.; Guilmet, E.; De Carvahlo, M.-E.; Poilblanc, R. *J. Am. Chem. Soc.* **1984**, *106*, 6668−6676.
(42) Johnson, D. W.; Margerum, D. W. *Inorg. Chem.* **1991**, *30*, 4845−4851.
(43) While this paper was being written, Meunier and co-workers published a correction to their original report (ref 41) that LiOCl exchanges slowly (B. Meunier et al., *J. Am. Chem. Soc.*, **2000**, *122*, 2675). Meunier suggests using peroxides, such as oxone, for unambiguous mechanistic detection of a Mn=O intermediate with $H_2{}^{18}O$.
(44) Irish, D. E.; Ozeki, T. *Raman Spectroscopy of Inorganic Species in Solution*; Wiley: New York, 1991; Vol. 114.
(45) Robert, A.; Meunier, B. *New J. Chem.* **1988**, *12*, 885−896.
(46) Reedy, B. J.; Bettie, J. K.; Lowson, R. T. *Spectrochim. Acta* **1990**, *46A*, 1513−1519.
(47) Hoering, T. C.; Kennedy, J. W. *J. Am. Chem. Soc.* **1958**, *79*, 56−60.
(48) Appleman, E. H.; Basile, L. J.; Kim, H.; Ferraro, J. R. *Spectrochim. Acta* **1985**, *41A*, 1295−1300.
(49) Maslowski, E., Jr. In *Vibrational Spectra of Organometallic Compounds*; Wiley: New York, 1977; p 422.
(50) Schugart, K. A.; Noblet, J. A. *J. Mol. Struct. (THEOCHEM)* **1994**, *304*, 13−26.

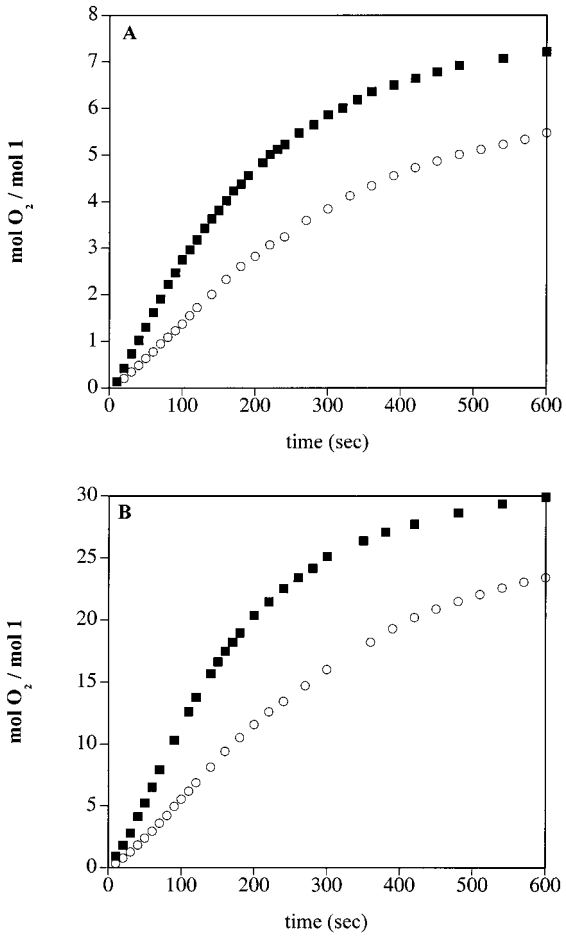

Figure 6. Plots showing turnovers vs time for the O_2-evolving reaction between HSO_5^- (0.23 M HOAc/OAc$^-$, pH = 4.5) and **1**; (A) [**1**] = 0.75 mM, $[HSO_5^-]$ = 15 mM in H_2O (filled squares) and D_2O (open circles); (B) [**1**] = 0.5 mM, $[HSO_5^-]$ = 50 mM in H_2O (filled squares) and D_2O (open circles).

reveals that the reactions are essentially complete in the first 10 min. The isotope effects were measured using the slope over the first few turnovers while still under pseudo-first-order conditions for oxone. When the mole ratio of HSO_5^-:**1** was 20:1, $k_H/k_D = 1.71 \pm 0.2$, and when the ratio was 100:1, $k_H/k_D = 1.64 \pm 0.02$. Although the ^{18}O-labeling experiments showed that, under these conditions, the O atoms in O_2 were derived primarily from water and oxone, respectively, the similar H/D isotope effects suggest that O_2 evolution has the same rate-limiting step under the two regimes. This indicates that the reaction pathway (water oxidation vs oxone/oxone coupling) is decided by the fate of the reaction intermediate. The apparent inverse isotope effect that appears after a few minutes is due to the faster consumption of oxidant in H_2O versus D_2O such that the reactions are no longer pseudo-first-order in oxone at later times.

An important issue is the fate of the complex during and after catalysis. We have addressed this issue by following the change in net oxidizing equivalents as a function of O_2 evolved and by using EPR and UV/vis spectroscopies to look at the species in solution during catalysis with HSO_5^-. When the III/IV dimer **1** is added to oxone, the solution turns darker green, the majority of the EPR-signal (>95%) for the III/IV dimer disappears (Figure 7), and there are no signals corresponding to monomeric Mn(II), II/II, or II/III species. After 1 h (the time-scale of the mass spectrometry experiment), 70% of the manganese is in the form of a III/IV dimer under conditions where the oxone is

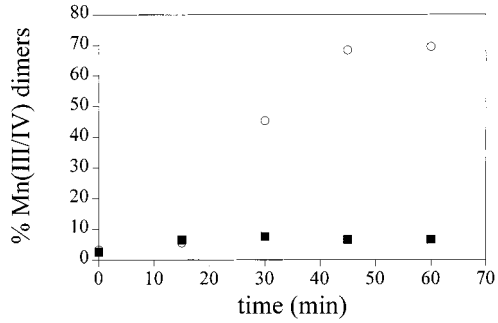

Figure 7. Plot of the amount of mixed-valence di-μ-oxo manganese dimer in solution (determined by EPR) as a function of time during catalysis with oxone. [**1**] = 0.75 mM, $[HSO_5^-]$ = 15 mM (open circles) and [**1**] = 0.5 mM, $[HSO_5^-]$ = 50 mM (filled squares).

almost fully consumed (Table 5).[51] Table 5 shows the number of oxidizing equivalents remaining in solution as a function of time. Importantly, O_2 evolution can account for ≥80% of the oxone consumed under both sets of conditions (Table 5), and so is the major reaction in solution. The reappearance of **1** upon consumption of oxone, coupled with O_2 evolution being the dominant reaction, shows that ligand oxidation is not a major factor.

Permanganate Formation. In the course of this study, we have found that the degree of deactivation of the catalyst by ligand loss and permanganate formation[14,15,33] is highly dependent on the relative concentrations of **1** and XO. When the ratio of XO:**1** is >500:1, most of **1** is converted to MnO_4^-, with isosbestic behavior.[14,15] However, MnO_4^- formation does not contribute significantly to the initial rates (<2% MnO_4^- formed in the first 30 s). On the other hand, no permanganate was detected over the time-course of O_2 evolution at the concentrations of **1** and oxone used for the mass spectrometry studies, where HSO_5^-:**1** is <100:1. This indicates that permanganate formation can be suppressed if bimolecular reactions of the Mn dimer occur instead. Furthermore, there is a deceleration of the rates of both O_2 evolution and MnO_4^- formation after just a few turnovers at high XO:**1** ratios (>500:1). We believe this could be due to anation of the dimer, as observed in the related $[(bpy)_2(H_2O)Ru^{III}(O)Ru^{III}(OH_2)(bpy)_2]^{4+}$ system,[16−18] or ligand loss. We are currently investigating these observations in greater detail, but will not consider the deactivating reactions further in this paper.

Discussion

Figure 8 shows a proposed mechanism for the formation of the reactive intermediate that is consistent with the experimental Michaelis−Menten kinetics, where the XO initially binds reversibly to **1**. The complex so formed (**3**) is analogous to **2** where sulfate can be thought of as a model for HSO_5^- binding to **1**. The mechanism is based upon the III/IV dimer being the reactive species, although other oxidation states cannot yet be ruled out (discussed below). Once formed, **3** can react with XO

(51) If the solution is left for long periods (>1 h) after the oxidant has been consumed, a brown precipitate of MnO_2 forms. If additional oxone is added, this solution can catalyze gas evolution at a rate much slower than that observed with **1** (data not shown). This means that any manganese complex that decomposes to MnO_2 could, in theory, react through a heterogeneous pathway. For catalysis with **1**, MnO_2 can be ruled out as the catalyst for O_2 formation at short reaction times because: (1) there is no lag period corresponding to MnO_2 formation, (2) the dimer stays intact under conditions where the oxone is consumed (shown in Figure 7), (3) no precipitate can be detected during the first 30 min of the reaction, and (4) the reaction is fastest in the presence of **1** and slows after the precipitate forms.

Table 5: Oxidizing Equivalents in Solution Per Mole of **1**

		10 min after addition of **1**			60 min after addition of **1**
conditions	before addition of **1**	O_2 evolved	remaining oxidizing equiv[a]	total	remaining oxidizing equiv[a]
50 mM oxone, 0.5 mM **1**	192	118 ± 2	36 ± 2	154	23 ± 1
15 mM oxone, 0.75 mM **1**	38.4	28.6 ± 0.4	4.4 ± 0.2	33.0	2.6 ± 0.2

[a] Corrected for the reduction of Mn(IV) in solution to Mn(II) upon addition of KI.

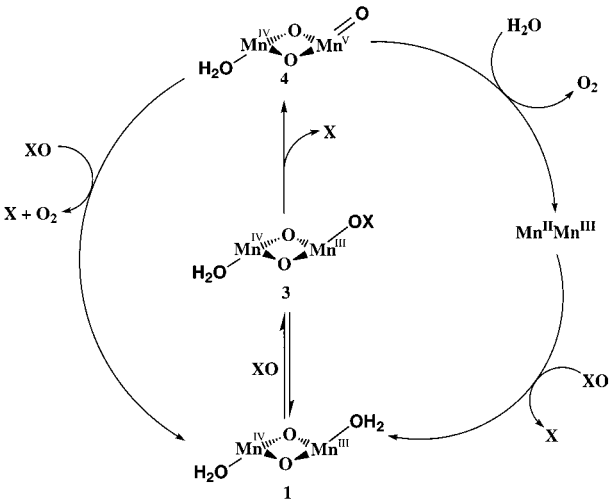

Figure 8. Proposed mechanism for the reaction between **1** and oxygen-atom transfer reagents, XO, based on findings in this paper and also previous studies.[14,15,33] In both cases, the rate-limiting step is formation of **4** by oxidation of **1**. While these mechanisms are mainly based on observations when HSO_5^- is used as the oxidant, the kinetic data we present in this study suggest that OCl^- most likely reacts in an analogous fashion. Left-hand pathway: attack of XO on the terminal oxo ligand of **4**. Right-hand pathway: attack of solvent H_2O on the terminal oxo ligand of **4**.

to form an intermediate containing a terminal Mn═O (**4**) (Figure 8), and this represents the rate-limiting step in O_2 evolution. It is unlikely that O_2 evolution involves a reaction between the **1**-XO complex and XO in solution, as this would give a second-order dependence of the initial rate on XO and would not explain the origin of $^{36}O_2$. Moreover, the kinetic data in Figure 3 cannot be fit by a rate law which involves such a mechanism.

Evidence for a Mn═O intermediate is provided by the ^{18}O-labeling experiments with $HS^{16}O_5^-$. The incorporation of ^{18}O from water into various organic products has been used in Mn-catalyzed oxidations to infer the presence of Mn═O intermediates.[21,22,29−31] The terminal oxo in **4** originates from oxone and thus would be ^{16}O initially but could exchange with labeled solvent via the mechanism shown in eq 1.

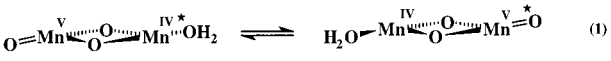

Equation 1 is clearly a simplified view as multiple protonation/depronation steps would be involved in the exchange.[29,30] The amount of label incorporated into the O_2 evolved would then depend on the relative rate of this exchange versus the O−O bond-forming step. A further possibility is that the exchange involves the bridging μ-oxo ligands and that they are involved in O−O bond formation. Such a mechanism has been proposed for the action of the OEC.[8,52,53]

Scheme 1. Possible Pathways for the Formation of Labeled and Unlabeled O_2 from the Reaction between **1** and $KHS^{16}O_5$ in $H_2{}^{18}O$ as Summarized in Table 4[a]

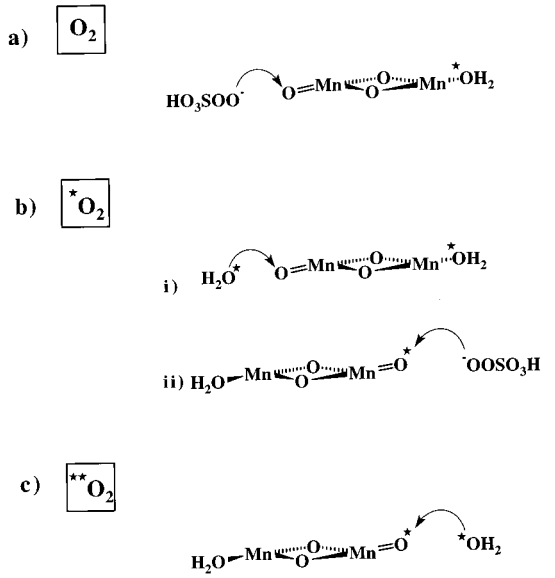

[a] The starred oxygens represent ^{18}O.

Scheme 1 shows mechanistic proposals that can account for each of the three isotopomers observed by mass spectrometry. $^{32}O_2$ could arise from the reaction of an unexchanged ^{16}O-oxo with oxone (Scheme 1a). The amount of unlabeled O_2 depends inversely on the concentration of oxone (Table 4), so that at lower oxone concentrations the rate of exchange (eq 1) becomes comparable to the rate of the oxone/oxo reaction. The $^{34}O_2$ could form from two pathways involving either attack of solvent water/hydroxide on an unexchanged Mn═O (Scheme 1b(i)) or an exchanged Mn═O reacting with free oxone (Scheme 1b(ii)). Finally, $^{36}O_2$ could arise from the reaction between solvent water and an exchanged Mn═O (Scheme 1c).

Certain inferences can be drawn from the labeling results. Multiple pathways must be invoked to account for the product distribution (Figure 8 and Scheme 1). At higher concentrations of HSO_5^- relative to that of **1**, the oxone/oxo pathway dominates (Figure 8, left-hand path) and is fast compared to exchange, and thus the major product is $^{32}O_2$ (Table 4). Again, a mechanism involving reaction between **1**-XO and XO in solution can be ruled out on the basis of the kinetics data (Figure 3) which show a first-order dependence on [XO]. However, as the oxone concentration is lowered, both the exchange reaction (eq 1) and the water/oxo reactions (Figure 8, right-hand path) become competitive with the oxone/oxo reaction and thus all three possible isotopomers, that is $^{32}O_2$, $^{34}O_2$, and $^{36}O_2$, are seen (Table 4). O_2 release from the reaction of **4** with solvent water would result in a II/III dimer. As no such species is observed by EPR, we presume that the II/III dimer intermediate is then rapidly reoxidized to **1** by oxone.

The oxidation state of the Mn complex responsible for catalysis is not yet known, and both the IV/IV and the III/IV states may be active. With both OCl^-[14] and HSO_5^- as oxidant,

(52) Halfen, J. A.; Mahapatra, S.; Wilkinson, E. C.; Kaderli, S.; Young, V. G.; Que, L.; Zuberbuhler, A. D.; Tolman, W. B. *Science* **1996**, *271*, 1397−1400.

(53) Pecoraro, V. L.; Baldwin, M. J.; Gelasco, A. *Chem. Rev.* **1994**, *94*, 807−826.

there is initially formation of a large amount (>95%) of an EPR-silent species that we attribute to a IV/IV dimer (probably formed by electron exchange between IV/V and III/IV species). Oxidation of a IV/IV dimer by oxone would most likely give a V/V dimer, where both manganese would have a terminal oxo ligand. As one of the terminal oxo ligands would have to come from water, even an oxone/oxo pathway (Figure 8, left, and Scheme 1a) would give labeled product. This is not seen, and for this reason, we propose that with oxone as oxidant, at least under the conditions of the ^{18}O-labeling experiments, the III/IV dimer is the active species. The observed D-isotope effect may partly arise from a perturbation of the initial equilibrium where D_2O exchanges slower than H_2O. In addition, oxidation of **3** to **4** may be accompanied by deprotonation of an aqua-ligand to minimize charge build-up on the complex, and this reaction would be expected to show a D-isotope effect.[14]

Conclusions

The data presented in this report show that **1** can catalyze water oxidation when HSO_5^- is used as a primary oxidant. The proposed mechanism involves an intermediate that can exchange with water and then react with water or oxone. We propose that this intermediate contains a formally $Mn^V{=}O$ and that the O−O bond-forming step involves attack of solvent or oxone on the oxo ligand. The kinetic studies show that **1** reacts with HSO_5^- and OCl^- by similar mechanisms. These results complement earlier work involving the reaction of **1** with OCl^-[14] and provide support for the mechanism shown in Figure 8. Our aim, now, is to try to isolate the reactive intermediates and to characterize further the species present during catalysis. These species may be analogous to those present in the OEC during turnover and thus will provide key insights into the mechanism of photosynthetic water oxidation.

Acknowledgment. We thank Professor Bernard Meunier for discussions on ^{18}O exchange, Mr. Michael Ranen for his assistance with the Raman instrumentation, and Susan de Gala for solving the crystal structure of **2**. Funding was provided by the National Institutes of Health GM32715 (G.W.B.) and by the Kresge Foundation (J.dP.).

Supporting Information Available: Tables containing detailed crystallographic data, atomic position parameters, bond lengths and bond angles of **2** (PDF). This material is available free of charge via the Internet at http://pubs.acs.org.

JA001090A